

Amide *Cis*–*Trans* Isomerization in Aqueous Solutions of Methyl *N*-Formyl-D-glucosaminides and Methyl *N*-Acetyl-D-glucosaminides: Chemical Equilibria and Exchange Kinetics

Xiaosong Hu,[†] Wenhui Zhang,[†] Ian Carmichael,[‡] and Anthony S. Serianni^{*,†}

Department of Chemistry and Biochemistry and Radiation Laboratory, University of Notre Dame, Notre Dame, Indiana 46556

Received October 12, 2009; E-mail: aseriann@nd.edu

Abstract: Amide *cis*–*trans* isomerization (CTI) in methyl 2-deoxy-2-acylamido-D-glucopyranosides was investigated by ¹H and ¹³C NMR spectroscopy. Singly ¹³C-labeled methyl 2-deoxy-2-formamido-D-glucopyranoside (MeGlcNFm) anomers provided standard ¹H and ¹³C chemical shifts and ¹H–¹³C and ¹³C–¹³C spin-coupling constants for *cis* and *trans* amides that are detected readily in aqueous solution. Equipped with this information, doubly ¹³C-labeled methyl 2-deoxy-2-acetamido-D-glucopyranoside (MeGlcNAc) anomers were investigated, leading to the detection and quantification of *cis* and *trans* amides in this biologically important aminosugar. In comparison to MeGlcNFm anomers, the percentage of *cis* amide in aqueous solutions of MeGlcNAc anomers is small (~23% for MeGlcNFm *versus* ~1.8% for MeGlcNAc at 42 °C) but nevertheless observable with assistance from ¹³C-labeling. Temperature studies gave thermodynamic parameters ΔG° , ΔH° , and ΔS° for *cis*–*trans* interconversion in MeGlcNFm and MeGlcNAc anomers. *Cis/trans* equilibria depended on anomeric configuration, with solutions of α -anomers containing less *cis* amide than those of β -anomers. Confirmation of the presence of *cis* amide in MeGlcNAc solutions derived from quantitative ¹³C saturation transfer measurements of CTI rate constants as a function of solution temperature, yielding activation parameters E_{act} , ΔG^{\ddagger} , ΔH^{\ddagger} , and ΔS^{\ddagger} for saccharide CTI. Rate constants for the conversion of *trans* to *cis* amide in MeGlcNFm and MeGlcNAc anomers ranged from 0.02 to 3.59 s⁻¹ over 31–85 °C, compared to 0.24–80 s⁻¹ for the conversion of *cis* to *trans* amide over the same temperature range. Energies of activation ranged from 16–19 and 19–20 kcal/mol for the *cis* → *trans* and *trans* → *cis* processes, respectively. Complementary DFT calculations on MeGlcNFm and MeGlcNAc model structures were conducted to evaluate the effects of an acyl side chain and anomeric structure, as well as C2–N2 bond rotation, on CTI energetics. These studies show that aqueous solutions of GlcNAc-containing structures contain measurable amounts of both *cis* and *trans* amides, which may influence their biological properties.

Introduction

Amide *cis*–*trans* isomerization (CTI) is an important exchange process in biological systems.¹ In proteins, especially those that are proline-rich (*e.g.*, collagen), the conformation of Xaa–Pro peptide bonds influences the pathway of protein folding and determines the final protein tertiary structure.² Prolyl *cis*–*trans* isomerases are well-known folding accessory proteins responsible for enzyme-catalyzed CTI of ^NXaa–Pro^C peptide bonds *in vivo*.³ Gly–Gly peptide bonds may also undergo spontaneous amide bond isomerization *in vivo* due to the

comparatively small energy difference between the *cis* and *trans* conformations caused by the absence of bulky R-groups.^{4,5} Recently, secondary amide peptide bond *cis*–*trans* isomerases (APIases) have been reported to catalyze amide CTI in nonprolyl peptide bonds; an example of this class of enzyme is the Hsp60 chaperone, DnaK.⁶ Amide CTI may also play a role in the chemo-mechanical cycle of motor proteins.⁷

Amide CTI in glycobiology is less prominent than in proteobiology, largely because glycosidic linkages are involved in the assembly of oligo/polysaccharides rather than peptide (amide) bonds. However, some biologically important saccharides contain amide bonds as part of a side chain substituent,

[†] Department of Chemistry and Biochemistry.

[‡] Radiation Laboratory.

(1) *cis*–*trans* Isomerization in Biochemistry; Dugave, C., Ed.; J Wiley & Sons: New York, 2006.

(2) (a) Stein, R. L. *Adv. Protein Chem.* **1993**, *44*, 1–24. (b) Schmid, F. X.; Mayr, L. M.; Mücke, M.; Schönbrunner, E. R. *Adv. Protein Chem.* **1993**, *44*, 25–66. (c) Hur, S.; Bruice, T. C. *J. Am. Chem. Soc.* **2002**, *124*, 7303–7313. (d) Agarwal, P. K.; Geist, A.; Gorin, A. *Biochemistry* **2004**, *43*, 10605–10618. (e) Fanghänel, J.; Fischer, G. *Front. Biosci.* **2004**, *9*, 3453–3478. (f) Lu, K. P.; Finn, G.; Lee, T. H.; Nicholson, L. K. *Nat. Chem. Biol.* **2007**, *3*, 619–629.

(3) Voet, D.; Voet, J. G. *Biochemistry*, 3rd ed.; J. Wiley & Sons: New York, 2004; p 290.

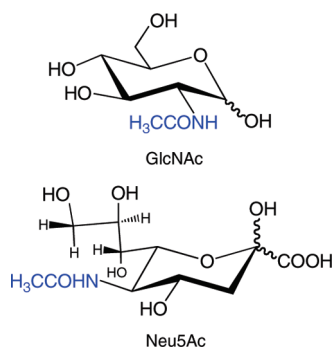
(4) Scherer, G.; Kramer, M. L.; Schutkowski, M.; Reimer, U.; Fischer, G. *J. Am. Chem. Soc.* **1998**, *120*, 5568–5574.

(5) Schiene-Fischer, C.; Fischer, G. *J. Am. Chem. Soc.* **2001**, *123*, 6227–6231.

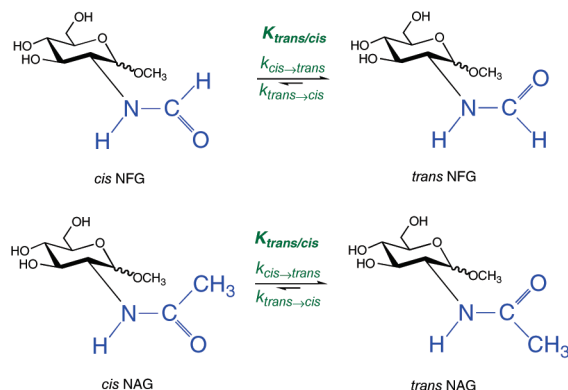
(6) Schiene-Fischer, C.; Habazettl, J.; Schmid, F. X.; Fischer, G. *Nat. Struct. Biol.* **2002**, *9*, 419–424.

(7) Tchaicheeyan, O. *FASEB J.* **2004**, *18*, 783–789.

Scheme 1



Scheme 2

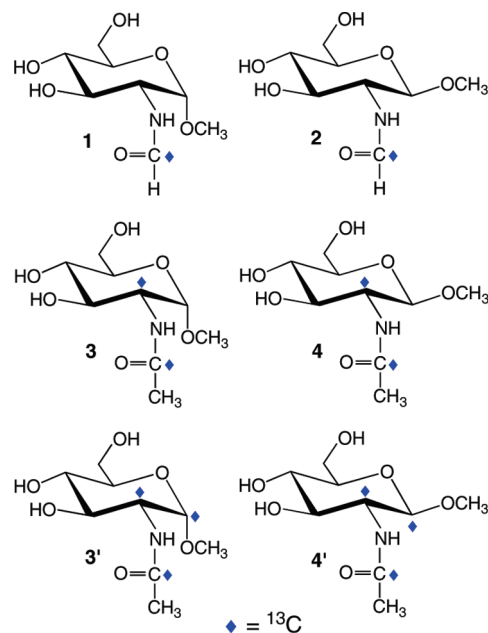


notably, the *N*-acetyl side chains of *N*-acetyl-D-glucosamine (GlcNAc; NAG) and *N*-acetylneuraminic acid (Neu5Ac) (Scheme 1). While it is commonly held that amide conformation in GlcNAc monomers is exclusively *trans*, it is known that, in some glycoprotein X-ray structures, NAG residues are observed with the *N*-acetyl side chain in the *cis* conformation.⁸ This observation led us to ponder whether the amide *cis*–*trans* equilibrium can be detected and quantified in aqueous solutions of methyl glycosides of GlcNAc and GlcNAc-related compounds (Scheme 2). In this report, we describe NMR approaches to detect and quantify *cis* and *trans* amides in aqueous solutions of these glycosides. Using saturation-transfer ¹³C NMR methods, first-order rate constants and kinetic activation parameters have been measured for CTI in saccharides. We show that the *cis*–*trans* equilibrium and exchange kinetics depend on saccharide anomeric configuration and side chain structure (*N*-acetyl *vs* *N*-formyl) (Scheme 2), demonstrating the importance of local structure on this side chain rearrangement.

Experimental Section

Methyl 2-Deoxy-2-[¹³C]formamido- α -D-glucopyranoside (1) (α -MeNFG) and Methyl 2-Deoxy-2-[¹³C]formamido- β -D-glucopyranoside (2) (β -MeNFG). 2-Acetamido-2-deoxy-D-glucose (3.00 g, 13.6 mmol) was dissolved in 30 mL of absolute MeOH, and Dowex HCR-W2 (H⁺) resin was added with gentle stirring. The reaction mixture was refluxed for 1 h, cooled, and filtered to remove the resin, and the filtrate was concentrated to a syrup at 30 °C *in vacuo* to give a crude mixture of glycoside anomers (2.87 g, 12.2 mmol). The syrup was dissolved in a minimal volume of H₂O, and the solution applied to a column (3.0 cm \times 50 cm) containing Dowex 1 \times 8 (200–400 mesh) (OH⁻) ion-exchange resin.^{9,10} The

column was eluted with distilled water at 2.7 mL/min, 20-mL fractions were collected, and the fractions were assayed for aminosugar using phenol-sulfuric acid.^{10,11} Methyl 2-acetamido-2-deoxy- α -D-glucopyranoside eluted first (fractions 17–19) (870 mg, 3.70 mmol, 27.2%), followed by methyl 2-acetamido-2-deoxy- β -D-glucopyranoside (fractions 21–25) (1.15 g, 4.89 mmol, 36.0%).



Methyl 2-acetamido-2-deoxy- α -D-glucopyranoside (830 mg, 3.53 mmol) was dissolved in 30 mL of H₂O, and barium oxide¹² was added batchwise to adjust the solution pH to \sim 13. The reaction mixture was refluxed for 12 h. After cooling to room temperature, the precipitate was removed by filtration, and the filtrate was treated with dry ice to precipitate barium salts. After filtration to remove the salts, the filtrate was concentrated to a syrup at 30 °C *in vacuo* to give methyl 2-amino-2-deoxy- α -D-glucopyranoside (677 mg, 3.53 mmol, 100%).

Methyl 2-amino-2-deoxy- α -D-glucopyranoside (670 mg, 3.47 mmol) was dissolved in a minimal volume of H₂O, and EtOH (25 mL) was added. Sodium [¹³C]formate (99 atom % ¹³C; Cambridge Isotope Laboratories, Inc.) (335 mg, 4.86 mmol, dissolved in 6 mL of H₂O) and EEDQ¹⁰ (2-ethoxy-1-ethoxycarbonyl-1,2-dihydroquinone) (857 mg, 3.47 mmol dissolved in 20 mL of EtOH) were added to the aminosugar solution with stirring. The reaction vessel was sealed with a rubber septum and covered with aluminum foil, and the solution was stirred at 30 °C for 24 h. The reaction mixture was then evaporated *in vacuo* at 30 °C to a syrup to remove ethanol and water. Distilled water (20 mL) was added to dissolve the aminosugar syrup, and the solution was extracted with 6 \times 15 mL of CH₂Cl₂. The resulting aqueous solution was deionized with batchwise additions of excess Dowex 50 \times 8 (20–50 mesh) (H⁺) and Dowex 1 \times 8 (20–50 mesh) (OAc⁻) ion-exchange resins. After filtration to remove the resins, the deionized filtrate was concentrated at 30 °C *in vacuo* to remove acetic acid. The crude methyl 2-deoxy-2-[¹³C]formamido- α -D-glucopyranoside (**1**) was purified by chromatography on a column (1.5 cm \times 68 cm) containing Dowex 50

(8) Bode, W.; Wei, A. Z.; Huber, R.; Meyer, E.; Travis, J.; Neumann, S. *EMBO J.* **1986**, *5*, 2453–2458.

(9) Austin, P. W.; Hardy, F. E.; Buchanan, J. C.; Baddiley, J. *J. Chem. Soc.* **1963**, 5350–5353.

(10) Zhu, Y.; Pan, Q.; Thibaudeau, C.; Zhao, S.; Carmichael, I.; Serianni, A. S. *J. Org. Chem.* **2006**, *71*, 466–479.

(11) Hodge, J. E.; Hofreiter, B. T. *Methods Carbohydr. Chem.* **1962**, *1*, 380–394.

(12) Neumann, J.; Weingarten, S.; Thiem, J. *Eur. J. Chem.* **2007**, 1130–1144. (These authors used Ba(OH)₂ octahydrate in this prior work; BaO was used as a substitute in the current work.)

× 8 (200–400 mesh) ion-exchange resin in the Ca²⁺ form¹³ to afford 560 mg (2.52 mmol, 72.6%) of **1**.

Methyl 2-deoxy-2-[¹³C]formamido-β-D-glucopyranoside (**2**) (β-MeNFG) was prepared by a procedure similar to that used for **1**. A detailed description is available in Supporting Information.

Methyl 2-[1-¹³C]Acetamido-2-deoxy-α-D-[2-¹³C]glucopyranoside (3) (α-MeNAG) and Methyl 2-[1-¹³C]Acetamido-2-deoxy-β-D-[2-¹³C]glucopyranoside (4) (β-MeNAG). 2-Amino-2-deoxy-D-[2-¹³C]glucose hydrochloride (400 mg, 1.85 mmol; Omicron Biochemicals, Inc.) was dissolved in a minimal volume of distilled H₂O, and the solution pH was adjusted to 6.6 with the addition of Dowex 1 × 8 (200–400 mesh) (OH[−]) ion-exchange resin. The resin was removed by filtration and washed with water, giving a total filtrate volume of ~6 mL to which was added 25 mL of EtOH. Sodium [1-¹³C]acetate (99 atom % ¹³C; Cambridge Isotope Laboratories, Inc.) (230 mg, 2.77 mmol, dissolved in a small amount of distilled H₂O) and EEDQ¹⁰ (2-ethoxy-1-ethoxycarbonyl-1,2-dihydroquinone) (684 mg, 2.77 mmol, dissolved in 10 mL of EtOH) were added to the aminosugar solution with stirring. The reaction vessel was sealed with a rubber septum and covered with aluminum foil, and the reaction solution was stirred at 30 °C for 24 h. The reaction solution was then concentrated *in vacuo* at 30 °C to a stiff syrup to remove ethanol and water. Distilled water (20 mL) was added to dissolve the syrup, and the solution was extracted with 6 × 15 mL of CH₂Cl₂. The resulting aqueous solution was deionized with batchwise additions of excess Dowex 50 × 8 (20–50 mesh) (H⁺) and Dowex 1 × 8 (20–50 mesh) (OAc[−]) ion-exchange resins, and the deionized solution was concentrated at 30 °C *in vacuo* to remove acetic acid. The crude yield of 2-[1-¹³C]acetamido-2-deoxy-D-[2-¹³C]glucopyranosides was 390 mg (1.75 mmol, 94.5%).

The 2-[1-¹³C]acetamido-2-deoxy-D-[2-¹³C]glucopyranosides (360 mg, 1.61 mmol) were dissolved in 30 mL of absolute MeOH, and Dowex HCR-W2 (H⁺) resin (~0.5 g) was added with gentle stirring. The reaction mixture was refluxed for 1 h, cooled, and filtered to remove the resin, and the filtrate was concentrated to a syrup of crude glycosides (300 mg, 1.27 mmol). The syrup was dissolved in a minimal volume of distilled H₂O, and the solution was applied to a column (3.0 cm × 50 cm) containing Dowex 1 × 8 (200–400 mesh) (OH[−]) ion-exchange resin.^{9,10} The column was eluted with distilled water at 2.7 mL/min, and 20-mL fractions were collected. Column fractions were assayed for aminosugar using a 1% (w/v) CeSO₄·2.5% (w/v) (NH₄)₆Mo₇O₂₄/10% aq H₂SO₄ reagent¹⁴ (fraction samples spotted on a silica gel TLC plate, followed by spraying with the reagent and charring on a hot plate). Methyl 2-[1-¹³C]acetamido-2-deoxy-α-D-[2-¹³C]glucopyranoside (**3**) eluted first (fractions 17–19) (98 mg, 0.414 mmol, 25.7%), followed by methyl 2-[1-¹³C]acetamido-2-deoxy-β-D-[2-¹³C]glucopyranoside (**4**) (fractions 21–25) (138 mg, 0.582 mmol, 36.1%).

Methyl 2-[1-¹³C]Acetamido-2-deoxy-α-D-[1,2-¹³C₂]glucopyranoside (3') (α-MeNAG) and Methyl 2-[1-¹³C]Acetamido-2-deoxy-β-D-[1,2-¹³C₂]glucopyranoside (4') (β-MeNAG). Compounds **3'** and **4'** were prepared by a procedure similar to that used for **3** and **4**. A detailed description is available in Supporting Information.

NMR Spectroscopy. Detection and Quantification of Amide *cis* and *trans* Isomers of 1–4 in Aqueous Solution. ¹³C NMR samples were prepared by dissolving ~20 mg of **1–4** in 0.7 mL of ²H₂O to give ~0.13 M solutions. The p²H values of the NMR solutions were adjusted to 8.1 ± 0.1 with Dowex HCR-W2 (H⁺) ion-exchange resin or dilute aqueous NaOH to eliminate potential effects of different [H⁺] on the measured equilibrium and rate constants.

The percentages of *cis* and *trans* forms in aqueous (²H₂O) solutions of **1–4** at different temperatures were determined by ¹³C{¹H} NMR spectroscopy (150 MHz ¹³C). Data acquisition and processing conditions were as follows: 90° pulse width; 36764.7

Hz spectral window, 20 s (1/2) and 30 s (3/4) relaxation delays, 1.8 s acquisition time. FIDs were treated with a 2-Hz exponential line-broadening function and were zero-filled once to give final spectral digital resolutions of ~0.14 Hz/pt. Peak areas of the *cis* and *trans* carbonyl or C2 resonances were determined by computer integration. Signals were carefully phased and starting and ending points selected to minimize integration errors. For each signal, the integration was performed three times, and the average value was used in the determination of solution percentages, from which *trans/cis* equilibrium constants, *K*_{*trans/cis*}, were calculated.

1D ¹H NMR spectra were obtained on a 600 MHz NMR spectrometer using a 90° pulse width, a spectral window of 9615.4 Hz, a relaxation delay of 0.6 s, and a 3.4 s acquisition time. FIDs were zero-filled twice to give final spectral digital resolutions of ~0.04 Hz/pt. 2D ¹H–¹H gCOSY¹⁵ and ¹³C–¹H gHSQC¹⁶ spectra were performed using standard NMR software to confirm ¹H and ¹³C signal assignments.

Measurement of CTI Rate Constants by ¹³C Saturation-Transfer NMR Spectroscopy. First-order rate constants for CTI in **1–4** were measured as a function of temperature by ¹³C saturation-transfer NMR (ST-NMR)^{17–20} using compounds **1–4** selectively labeled with ¹³C at the carbonyl carbon of the *N*-acyl side chain and/or the C2 ring carbon.

$$cis\ amide \xrightleftharpoons[k_{trans \rightarrow cis}]{k_{cis \rightarrow trans}} trans\ amide$$

The Bloch equation, modified to account for chemical exchange and describing the change in intensity (*M_z*) of the carbonyl carbon (or C2) resonance as a function of time, *t*, after the application of a nonselective 90° pulse, is as follows:

$$\frac{dM_z^{trans}}{dt} = \frac{-[M_z^{trans}(t) - M_z^{trans}(0)]}{T_{1,trans}} - k_{trans \rightarrow cis} M_z^{trans}(t) + k_{cis \rightarrow trans} M_z^{cis}(t) \quad (1)$$

Single-resonance saturation experiments were conducted at 150 MHz (¹³C). The selected *cis* resonance was saturated for times ranging from 0.005 to 50 s before application of a 90° observe pulse, and a relaxation delay of 20–30 s was used to allow for complete relaxation. In the saturation-transfer experiment, the *cis* resonance, denoted *M_z^{cis}*, is saturated, which causes *M_z^{cis}* → 0 and thus *k*_{*cis*→*trans*}*M_z^{cis}*(*t*) → 0. The resulting equation containing terms for *M_z^{trans}*, *T*_{1,*trans*}, and *k*_{*trans*→*cis*} can be integrated to the following form:

$$M_z^{trans}(\tau) = M_z^{trans}(0) \left(\frac{\tau_{1,trans}}{\tau_{trans}} \exp\left(\frac{-\tau}{\tau_{1,trans}}\right) + \frac{\tau_{1,trans}}{T_{1,trans}} \right) \quad (2)$$

where *M_z^{trans}*(*τ*) is the intensity of the *trans* resonance at time *τ* after onset of saturation of the *cis* resonance, and *M_z^{trans}*(0) is the intensity of the *trans* resonance in the absence of saturation. Furthermore,

- (15) (a) von Kienlin, M.; Moonen, C. T. W.; van der Toorn, A.; van Zijl, P. C. M. *J. Magn. Reson.* **1991**, *93*, 423–429. (b) Canet, D. *Prog. NMR Spectrosc.* **1997**, *30*, 101–135.
 (16) (a) Vuister, G. W.; Boelens, R.; Kaptein, R.; Hurd, R. E.; John, B.; van Zijl, P. C. M. *J. Am. Chem. Soc.* **1991**, *113*, 9688–9690. (b) Kay, L. E.; Keifer, P.; Saareinen, T. *J. Am. Chem. Soc.* **1992**, *114*, 10663–10665.
 (17) Forsén, S.; Hoffman, R. A. *J. Chem. Phys.* **1963**, *39*, 2892–2901.
 (18) Campbell, I. D.; Dobson, C. M.; Ratcliffe, R. G.; Williams, R. J. P. *J. Magn. Reson.* **1978**, *29*, 397–417.
 (19) Serianni, A. S.; Pierce, J.; Huang, S.-G.; Barker, R. *J. Am. Chem. Soc.* **1982**, *104*, 4037–4044.
 (20) Snyder, J. R.; Johnston, E. R.; Serianni, A. S. *J. Am. Chem. Soc.* **1989**, *111*, 2681–2687.

(13) Angyal, S. J.; Bethell, G. S.; Beveridge, R. J. *Carbohydr. Res.* **1979**, *73*, 9–18.

(14) Tropper, F. D.; Andersson, F. O.; Grand-Maitre, C.; Roy, R. *Carbohydr. Res.* **1992**, *229*, 149–154.

$$\frac{1}{\tau_{1,trans}} = \frac{1}{\tau_{trans}} + \frac{1}{T_{1,trans}} \quad (3)$$

where $\tau_{trans} = 1/k_{trans \rightarrow cis}$ and $T_{1,trans}$ is the spin–lattice relaxation time of the *trans* resonance.

For **3** and **4** (MeNAG anomers), the small percentage of *cis* form in solution at equilibrium (<3%) allowed for rapid (*i.e.*, within 0.005 s) and selective saturation of the *cis* C1' (carbonyl) carbon resonance. Consequently, $k_{trans \rightarrow cis}$ was measured from a plot of $\ln(M_z^{trans}(\tau) - M_z^{trans}(\infty))$ versus saturation time τ , where $M_z^{trans}(\infty)$ is the intensity of the *trans* C1' carbon resonance an “infinite” time (defined as $5(k_{trans \rightarrow cis} + 1/T_{1,trans})^{-1}$ after applying the saturating irradiation, giving a line with slope = $-1/\tau_{1,trans}$. The relaxation time was determined from the relationship

$$\frac{M_z^{trans}(\infty)}{M_z^{trans}(0)} = \frac{\tau_{1,trans}}{T_{1,trans}} \quad (4)$$

The values of $M_z^{trans}(0)$ and $M_z^{trans}(\infty)$ were determined using τ values of 0.005 and 50 s, respectively. Therefore, both $\tau_{1,trans}$ and $T_{1,trans}$ could be computed with precision, and eq 3 applied to determine τ_{trans} . From τ_{trans} , the rate constant $k_{trans \rightarrow cis}$ was calculated. From the $K_{trans/cis}$ equilibrium constant and $k_{trans \rightarrow cis}$ at a given temperature, $k_{cis \rightarrow trans}$ was determined.

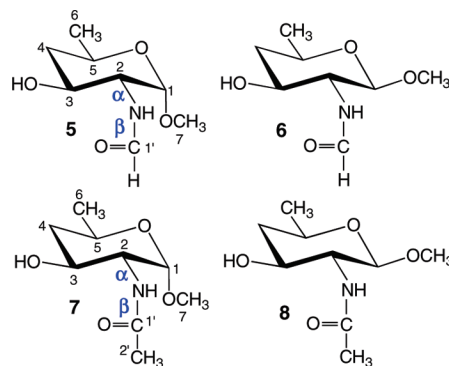
For **1** and **2** (MeNFG anomers), the relatively large percentage of *cis* form in solution (~20%) prevented rapid and selective saturation of the *cis* signal within a short time period (*i.e.*, 0.005 s). Therefore a different procedure was followed to determine $k_{trans \rightarrow cis}$ values. The $M_z^{trans}(\infty)/M_z^{trans}(0)$ ratio was determined by conducting two saturation transfer experiments with identical saturation times (20 s), with saturation at the *cis* carbonyl carbon resonance frequency (on-resonance) in the first experiment and with saturation at a frequency far from all other resonances in the spectrum (130 ppm; off-resonance) in the second. A relaxation delay of 20 s was used in both experiments. These two experiments yielded the ratio, $M_z^{trans}(\infty)/M_z^{trans}(0)$. $T_{1,trans}$ was then determined directly via an inversion–recovery experiment.^{21,22} With $M_z^{trans}(\infty)/M_z^{trans}(0)$ and $T_{1,trans}$ available, $\tau_{1,trans}$ was determined from eq 4, and τ_{trans} determined from eq 3. From τ_{trans} , $k_{trans \rightarrow cis}$ was calculated. Using the equilibrium constant measured at the same temperature, $k_{cis \rightarrow trans}$ was calculated.

Values of E_{act} , ΔG^{\ddagger} , ΔH^{\ddagger} , and ΔS^{\ddagger} for *cis*→*trans* and *trans*→*cis* reactions of **1**–**4** were calculated as described in Supporting Information.

Calculations

Geometry optimizations were conducted with the use of Gaussian03,²³ and density functional theory (DFT) was employed with the B3LYP functional²⁴ and the 6-31G* basis set²⁵ (B3LYP/6-31G*). The effect of solvent water was evaluated using the self-consistent reaction field (SCRFF),²⁶ the integral equation formalism (polarizable continuum) model (IEFPCM),²⁷ and the above-noted B3LYP/6-31G* computational method as implemented in Gaussian03. The united atom topological model (UAHF)²⁸ was applied

in the calculation by using RADII=UAHF in the input file to ensure convergence during energy minimization.



Model structures **5**–**8** were used to mimic compounds **1**–**4**, respectively. Calculations were conducted on **5**–**8** in two limiting conformations about α , defined as the H2–C2–N2–H torsion angle; these conformations are denoted α -*syn* and α -*anti*. In both α conformations, the β torsion angle, defined as H–N2–C1'–O in **5/6** and C2–N2–C1'–C2' in **7/8**, was rotated in 15° increments through 360°, giving a total of 24 optimized structures each for **5**–**8** (total of 96 optimized structures). Exocyclic torsion angles in both α -*syn* and α -*anti* forms were constrained as follows: the C2–C1–O1–C7 and the C2–C3–O3–H torsion angles were fixed at 180°. In addition, the C3–C2–N2–C1' torsion angle was fixed at 60° for α -*syn* and –120° for α -*anti*, the C1–C2–N2–C1' torsion angle was fixed at –60° for α -*syn* and 120° for α -*anti*, and the H2–C2–N2–H torsion angle was fixed at 0° for α -*syn* and 180° for α -*anti*. All other geometric parameters were allowed to optimize. Energy data obtained for **5/6** and **7/8** were normalized within each pair; for example, the lowest energy structure within the GlcNAc series was **7** (solvated) in the α -*anti* conformation with a C2–N2–C1'–C2' torsion angle of 180° (*trans* amide). The total energy of this structure was arbitrarily set at 0 kcal/mol, and the energies of the remaining 95 structures within the series are reported relative to this reference structure. Data for **5/6** were treated similarly.

Results and Discussion

General Experimental Strategy. The primary aim of this investigation was to determine whether both *cis* and *trans* amide conformations of GlcNAc glycosides **3** and **4** are detectable in aqueous solution by NMR spectroscopy. It was expected that very minor amounts of the *cis* form would be present, making its identification by NMR difficult (*i.e.*, weak signals might arise from the presence of contaminants rather than from the *cis* isomer). To address these concerns, methyl glycosides of *N*-formyl derivatives **1** and **2** were prepared, since prior work had shown that *cis* and *trans* amides coexist in aqueous solution in comparable amounts in related structures.^{29–32} Our underlying assumption was that the effects of amide conformation on the ¹³C chemical shifts of **3** and **4** would be similar to those observed in **1** and **2**. In addition, **3** and **4** were prepared with ¹³C-labeling

- (21) Vold, R. L.; Waugh, J. S.; Klein, M. P.; Phelps, D. E. *J. Chem. Phys.* **1968**, *48*, 3831–3832.
 (22) Weiss, G. H.; Ferretti, J. A. *Prog. NMR Spectrosc.* **1988**, *4*, 317–335.
 (23) Frisch, M. J.; et al. *Gaussian03, Revision A.1*; Gaussian, Inc.: Pittsburgh, PA, 2003.
 (24) Becke, A. D. *J. Chem. Phys.* **1993**, *98*, 5648–5652.
 (25) Hehre, W. J.; Ditchfield, R.; Pople, J. A. *J. Chem. Phys.* **1972**, *56*, 2257–2261.
 (26) Cancés, M. T.; Mennucci, B.; Tomasi, J. *J. Chem. Phys.* **1997**, *107*, 3032–3041.
 (27) Cammi, R.; Mennucci, B.; Tomasi, J. *J. Phys. Chem. A* **2000**, *104*, 5631–5637.
 (28) Barone, V.; Cossi, M.; Tomasi, J. *J. Chem. Phys.* **1997**, *107*, 3210–3221.

- (29) Katzenellenbogen, E.; Romanowska, E.; Kocharova, N. A.; Shashkov, A. S.; Knirel, Y. A.; Kochetkov, N. K. *Carbohydr. Res.* **1995**, *273*, 187–195.
 (30) Muldoon, J.; Shashkov, A. S.; Senchenkova, S. N.; Tomshich, S. V.; Komandrova, N. A.; Romanenko, L. A.; Knirel, Y. A.; Savage, A. V. *Carbohydr. Res.* **2001**, *330*, 231–239.
 (31) Kocharova, N. A.; Maszewska, A.; Zatonsky, G. V.; Bystrova, O. V.; Ziolkowski, A.; Torzewska, A.; Shashkov, A. S.; Knirel, Y. A.; Rozalski, A. *Carbohydr. Res.* **2003**, *338*, 1425–1430.
 (32) Breazeale, S. D.; Ribeiro, A. A.; McClerren, A. L.; Raetz, C. R. H. *J. Biol. Chem.* **2005**, *280*, 14154–14167.

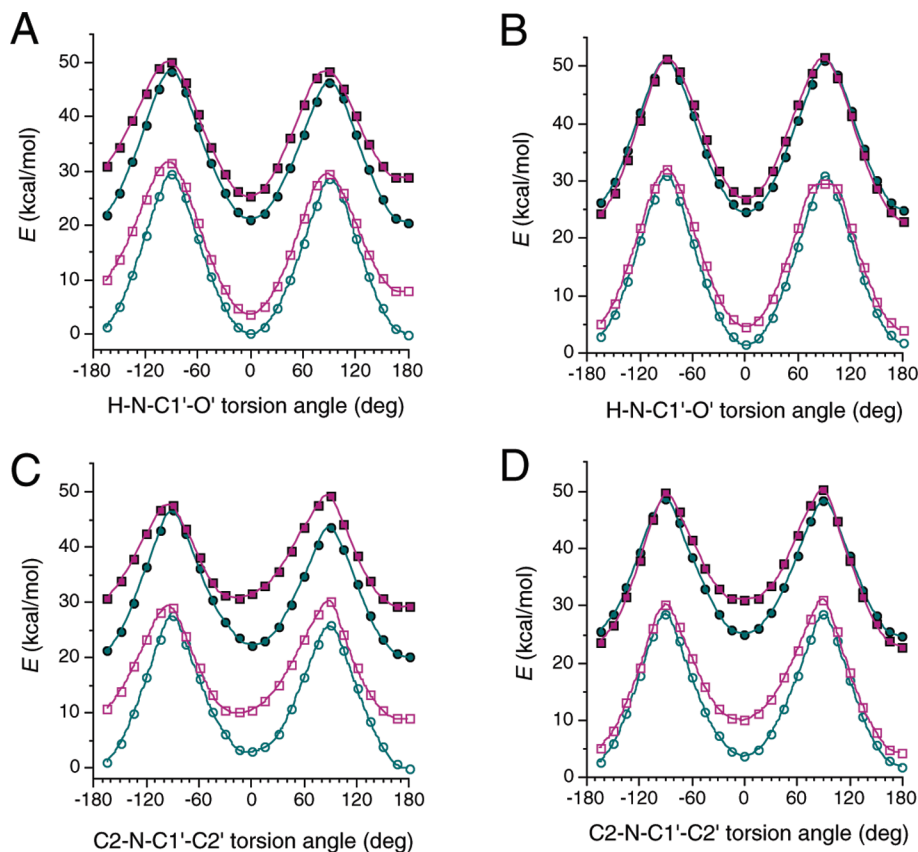


Figure 1. DFT-calculated total energies for **5** (A), **6** (B), **7** (C), and **8** (D) as a function of rotation of the N2–C1' amide bond (0° = pure *cis*; 180° = pure *trans*). Solid symbols = *in vacuo* energies; open symbols = solvated energies. Red symbols = α -*syn*; green symbols = α -*anti*.

at both C2 and C1' (the side chain carbonyl carbon) to allow detection of the geminal $^2J_{C_2,C_1'}$ spin-coupling constant between the labeled carbons. Observation of internally consistent $^2J_{C_2,C_1'}$ splitting patterns would thus provide further evidence for the *cis* isomer, because weak signals from contaminants would likely show either no splitting or a splitting pattern different from that expected. Upon detection of signals attributable to a putative *cis* isomer based on chemical shift and J_{CC} arguments, ^{13}C -labeling at either the side chain carbonyl carbon or the C2 ring carbon would then be exploited in quantitative ^{13}C saturation-transfer experiments to confirm the presence of *cis* \rightleftharpoons *trans* chemical exchange and allow measurements of first-order rate constants as a function of temperature, from which kinetics parameters could be determined. The magnitude of the latter values would provide indirect evidence for *cis* \rightleftharpoons *trans* equilibria in solution, since these parameters have been measured previously in related systems.^{4,5,33}

Synthesis of ^{13}C -labeled GlcNAc methyl glycosides was accomplished using methods described previously.¹⁰ 2-Amino-2-deoxy-D-glucose was converted to its 2-deoxy-2-acetamido derivative using sodium acetate and EEDQ. The resulting *N*-acetyl-D-glucosamine was subsequently converted to an anomeric mixture of methyl glycopyranosides, and the glycosides were separated by chromatography. D-[1- ^{13}C]Glucosamine, D-[1,2- $^{13}\text{C}_2$]glucosamine, and/or sodium [1- ^{13}C]acetate were used in the protocol to give two sets of ^{13}C -isotopomers **3/4** and **3'/4'**.

Synthesis of the methyl glycosides of NFG was less straightforward. Attempts to glycosidate *N*-formyl-D-glucosamine led

to substantial amide hydrolysis (Scheme S1, Route A; see Supporting Information). Consequently, an alternate route was followed (Scheme S1, Route B; see Supporting Information) in which GlcNAc was first converted to its methyl glycopyranosides and the latter were hydrolyzed with aqueous BaO to give intermediate glycosides of the free amine. The latter hydrolysis occurred relatively smoothly and in reasonable yield. The free amine glycosides were then converted to the *N*-formyl derivatives using sodium [^{13}C]formate and EEDQ, and the glycopyranoside anomers were purified by chromatography.

Energies of the *Cis* and *Trans* Isomers of **5–**8**.** DFT-Derived energies of **5**–**8** as a function of conformation about the α and β bonds are shown in Figure 1 and are summarized in Table S1 (see Supporting Information). *In vacuo* and solvated energies were calculated and compared (Figure 1). Inclusion of solvent lowered absolute energies significantly as expected, but relative energies were largely unchanged. Activation barriers for the interconversion of *cis* and *trans* isomers range from 18 to 29 kcal/mol, and in most but not all cases, inclusion of solvent enhanced the barriers. Activation barriers for *cis* \rightarrow *trans* differ slightly depending on the pathway of rotation, since the system is asymmetric. In general, barriers are slightly higher for the $-90^\circ \rightarrow 180^\circ$ pathway than for the $90^\circ \rightarrow 180^\circ$ pathway in **5/6**; for **7/8**, no general pattern emerges from the data (Table S1). Experimental energies of activation (E_{act}) for *cis* \rightarrow *trans* of 65–82 kJ/mol (15.5–19.6 kcal/mol) have been reported previously for the peptide bonds of oligopeptides.⁴

Within the solvated data set for MeNFG anomers, the most stable structure was **5** (α -*anti*) in the *trans* amide conformation, followed closely by **5** (α -*anti*) [$+0.06$ kcal/mol] (*cis* amide), **6** (α -*anti*)

(33) Wawra, S.; Fischer, G. In *cis-trans Isomerization in Biochemistry*; Dugave, C., Ed.; J. Wiley & Sons: New York, 2006; pp 167–193.

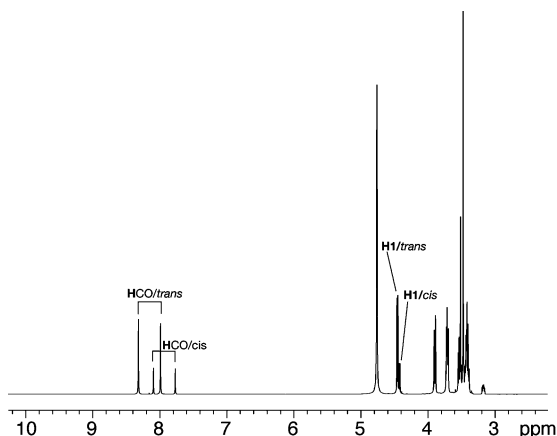


Figure 2. 600 MHz ^1H NMR spectrum of **2** in $^2\text{H}_2\text{O}$ at 22 °C showing signals arising from the anomeric H1 and side chain formyl hydrogen in the *cis* and *trans* forms of the molecule. The formyl hydrogen signals appear as doublets as a result of the presence of one-bond ^{13}C – ^1H spin-coupling involving the ^{13}C -labeled formyl carbon ($^1J_{\text{CH}} = 195.6$ Hz (*cis* isomer) and 197.7 Hz (*trans* isomer)).

[+1.37 kcal/mol] (*cis* amide), and **6** (α -*anti*) [+1.70 kcal/mol] (*trans* amide). For MeNAG anomers, the most stable structure was **7** (α -*anti*) in the *trans* amide conformation, followed closely by **8** (α -*anti*) (+1.98 kcal/mol (*trans* amide)). The latter findings are consistent qualitatively with NMR data showing a greater proportion of *N*-acetyl- α -D-glucosamine than *N*-acetyl- β -D-glucosamine (68% α -pyranose; 32% β -pyranose) in aqueous solution and with the commonly held assumption that α -*anti* conformations are more stable than α -*syn* conformations in GlcNAc anomers based on magnitudes of $^3J_{\text{H}_2\text{N}_\text{H}}$ values.^{34,35} In MeNFG models **5** and **6**, α -*anti* structures appear favored in both anomers, but a more balanced distribution of *cis* and *trans* amide conformations is predicted in these structures. It should be noted, however, that these energy calculations will be influenced by subtle intramolecular H-bonding involving side chain atoms and adjacent OH groups at C1 and C3, which can skew energies in favor of forms that are not significantly populated in solution, although the inclusion of a polarizable dielectric continuum in the calculation probably mitigates this effect to some extent. In addition, the present calculations explore a limited set of exocyclic C–O bond torsions in the vicinity of the *N*-formyl/*N*-acetyl side chain, and thus only portions of the full energy hypersurfaces were sampled. Therefore, although the calculations yield reasonable *cis*–*trans* interconversion barriers, relative stabilities of pyranose anomers, and conformational behavior about α , they are not expected to yield quantitative energies of *cis* and *trans* isomers and thus accurate *cis/trans* equilibria.

NMR Spectra of 1 and 2. 1D ^1H NMR spectra of **1** and **2** show the presence of *cis* and *trans* forms of each molecule in aqueous solution (Figure 2; Table 1; for ^1H – ^1H and ^{13}C – ^1H spin-couplings, see Table S2 in Supporting Information). ^1H nuclei most affected by amide conformation are H1, H2, H3, OCH₃, and the formyl hydrogen, with the largest effect observed at H2 (~0.5 ppm), followed by the formyl hydrogen (0.1–0.2 ppm) (Table 1). The direction of chemical shift changes observed upon the conversion of *trans* → *cis* varies with proton site and anomeric configuration. The H2, H3, and formyl hydrogen signals shift upfield, whereas the H1 and OCH₃ signals shift downfield in **1**; similar behavior is found for **2**, except in this case H1 shifts upfield. In contrast, the chemical shifts of H4–H6a/H6b in **1/2** are minimally affected by amide conformation (changes < 0.03 ppm). Presumably these

effects are caused by the shielding anisotropy of the exocyclic carbonyl group, with its influence on nearby ^1H shifts determined by differences in the orientation of the C=O bond relative to specific ring protons. Ring protons remote from the side chain are less subject to this effect, and the small shift changes observed may be due to subtle effects on ring molecular orbitals mediated by amide conformation and/or small changes in pyranosyl ring conformation.

Virtually all ^{13}C NMR signals in **1** and **2** are affected by amide conformation (Figure 3; Table 1; for ^{13}C – ^{13}C spin-couplings, see Table 3). The largest differences upon conversion of *trans* → *cis* are observed at C2 and the exocyclic formyl carbon (~4.7 and ~3.2 ppm downfield shifts, respectively).

In summary, NMR data obtained on the NFG methyl glycosides reveal chemical shift dependencies on side chain amide conformation that will be exploited in the following analyses of NMR data obtained on the NAG methyl glycosides **3** and **4**. The underlying assumption is that the direction of ^1H and/or ^{13}C chemical shift changes observed in **1/2** and their magnitudes will be similar to those in **3/4**.

The large difference in ^{13}C chemical shifts of the formyl (C1') carbon in the *cis* and *trans* forms and the presence of ^{13}C -labeling at C1' facilitated measurements of $K_{\text{trans/cis}}$ in **1** and **2** at different solution temperatures (Table 2). $K_{\text{trans/cis}}$ is affected by anomeric configuration; at all temperatures studied, the percentage of *cis* form in solution is greater in β -anomer **2** than in α -anomer **1**. For example, at 42°, $K_{\text{trans/cis}}$ is 4.22 ± 0.03 for **1** and 2.84 ± 0.02 for **2**, translating into ~19% *cis* for **1** and ~26% *cis* for **2**. van't Hoff plots of the data in Table 2 (see Figure S1 in Supporting Information) gave the following standard enthalpy changes, $\Delta H^\circ_{\text{cis} \rightarrow \text{trans}}$, for the conversion of *cis* to *trans* forms: -1.1 ± 0.1 kcal/mol for **1**; -0.8 ± 0.1 kcal/mol for **2**. $\Delta H^\circ_{\text{cis} \rightarrow \text{trans}}$ and standard entropy changes, $\Delta S^\circ_{\text{cis} \rightarrow \text{trans}}$, were determined from van't Hoff plots and used to calculate standard free energy changes, $\Delta G^\circ_{\text{cis} \rightarrow \text{trans}}$: $\Delta G^\circ_{\text{cis} \rightarrow \text{trans}}$ and $\Delta S^\circ_{\text{cis} \rightarrow \text{trans}}$ for **1**, -0.9 ± 0.1 kcal/mol and -0.8 ± 0.3 cal/K/mol; for **2**, -0.7 ± 0.1 kcal/mol and -0.6 ± 0.2 cal/K/mol. In **1** and **2**, the conversion of *cis* → *trans* amide is enthalpically favored but entropically disfavored, explaining the observed temperature dependence of $K_{\text{trans/cis}}$ (higher temperatures reduce $K_{\text{trans/cis}}$ and increase the percentage of *cis* form in solution).

^{13}C NMR spectra of **1** and **2** yielded J_{CC} values involving the side chain ^{13}C -labeled formyl carbon (C1') and the natural abundance carbons of the pyranosyl ring; these spin-couplings include $^2J_{\text{C}_2\text{C}_1'}$, $^3J_{\text{C}_1\text{C}_1'}$, and $^3J_{\text{C}_3\text{C}_1'}$ (Figure 3, Table 3). While the latter two couplings are expected to depend strongly on C2–N2 bond conformation (Karplus dependency) and thus can vary appreciably in magnitude in different structures, the geminal $^2J_{\text{C}_2\text{C}_1'}$ is likely to be less structure-sensitive and thus serves as a more reliable probe in the assignment of weak signals arising from *cis* forms in ^{13}C NMR spectra of **3** and **4**. For this reason, **3** and **4** were prepared each with two sites of ^{13}C enrichment to detect the C=O (C1') and C2 signals selectively;

(34) (a) Horton, D.; Jewell, J. S.; Philips, K. D. *J. Org. Chem.* **1966**, *31*, 4022–4025. (b) Neuberger, A.; Fletcher, A. P. *Carbohydr. Res.* **1971**, *17*, 79–88. (c) Two arguments have been offered to explain the predominant α -anomeric configuration of GlcNAc in aqueous solution. The first invokes a dipole–dipole interaction between the C1–O1 and the amide C=O bonds that is minimized in the α -pyranose.^{34b} The second invokes hydrogen-bonding between the amide NAc side chain hydrogen and O1 as a means of preferentially stabilizing the α -pyranose (*cis*-fused five-membered ring).^{34a} Both arguments presume an approximate α -*anti*/ β -*trans* conformation of the NAc side chain in GlcNAc.

Table 1. ^1H and ^{13}C Chemical Shift Assignments^a for **1** and **2** in Their *Cis* and *Trans* Amide Conformations

cmpd	$\delta_{\text{H}1}$	$\delta_{\text{H}2}$	$\delta_{\text{H}3}$	$\delta_{\text{H}4}$	$\delta_{\text{H}5}$	$\delta_{\text{H}6a}$	$\delta_{\text{H}6b}$	δ_{OCH_3}	δ_{COH}
1 / <i>β-cis</i>	4.797	~3.47	3.61–3.66	3.421	3.61–3.66	~3.84	3.741	3.369	7.970
1 / <i>β-trans</i>	4.747	3.964	3.669	3.450	3.61–3.66	3.840	3.744	3.357	8.103
2 / <i>β-cis</i>	4.423	3.172	3.504	3.37–3.45	3.37–3.45	3.895	3.708	3.514	7.931
2 / <i>β-trans</i>	4.454	3.714	3.535	3.37–3.45	3.37–3.45	3.895	3.708	3.472	8.153

cmpd	$\delta_{\text{C}1}$	$\delta_{\text{C}2}$	$\delta_{\text{C}3}$	$\delta_{\text{C}4}$	$\delta_{\text{C}5}$	$\delta_{\text{C}6}$	δ_{OCH_3}	$\delta_{\text{C=O}}$
1 / <i>β-cis</i>	101.48	59.52	73.72	72.17	74.27	63.07	57.74	170.07
1 / <i>β-trans</i>	100.61	54.77	73.77	72.39	74.30	63.10	57.69	166.96
2 / <i>β-cis</i>	104.00	61.56	75.94	72.27	78.41	63.21	59.98	170.68
2 / <i>β-trans</i>	104.28	56.82	76.23	72.44	78.47	63.27	59.69	167.33

^a ^1H chemical shifts in ppm relative to external dimethyl-2-silapentane-5-sulfonic acid (DSS); ^{13}C chemical shifts in ppm relative to external DSS. Measured at 22 °C in $^2\text{H}_2\text{O}$.

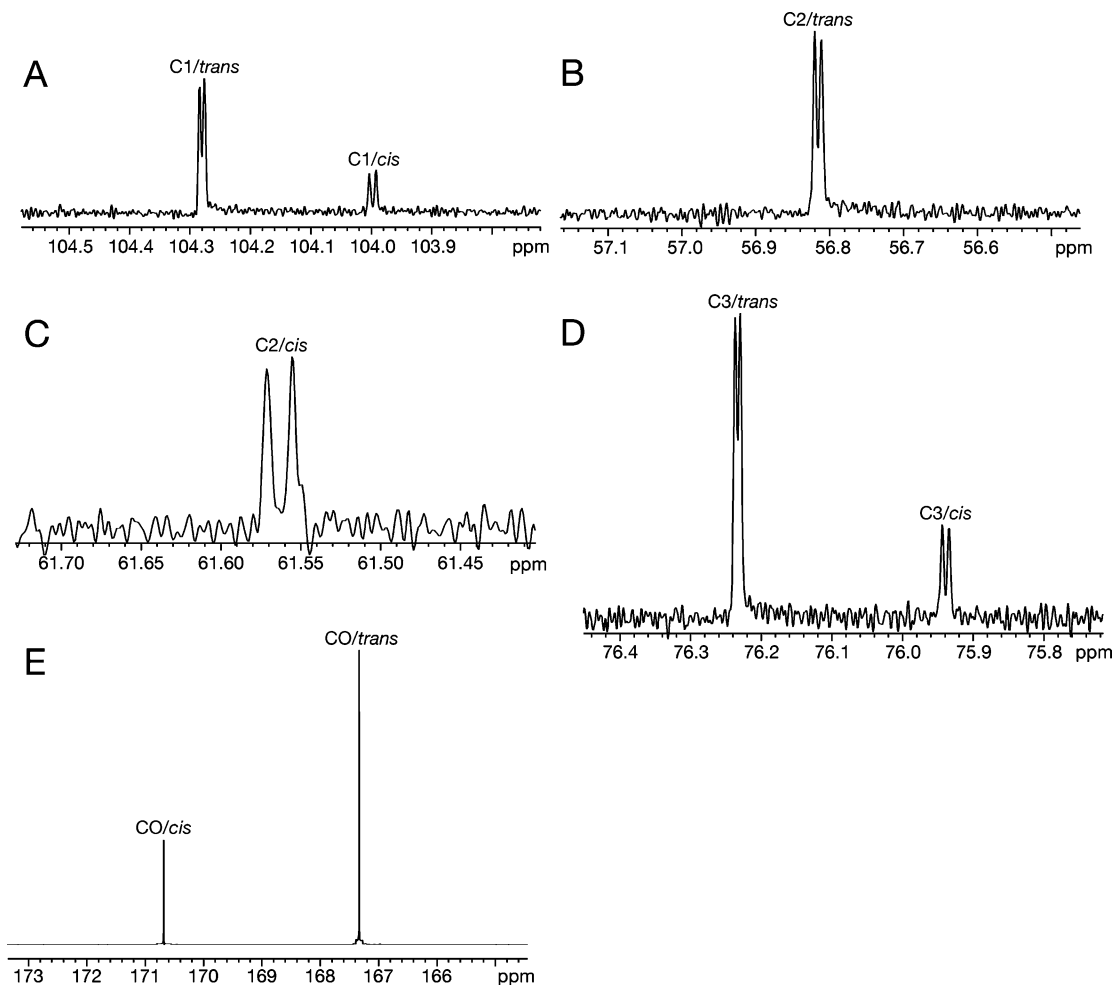


Figure 3. Partial $^{13}\text{C}\{^1\text{H}\}$ NMR spectra (150 MHz) of **2** in $^2\text{H}_2\text{O}$ at 22 °C. (A) Anomeric C1 signals in the *cis* and *trans* amides, showing splittings due to $^3J_{\text{C}1,\text{C}1'}$. (B, C) C2 signals in the *cis* and *trans* amides, showing splittings due to $^2J_{\text{C}2,\text{C}1'}$. (D) C3 signals in the *cis* and *trans* amides showing splittings due to $^3J_{\text{C}3,\text{C}1'}$. (E) Intense signals from the labeled formyl (C1') carbon in the *cis* and *trans* amides. See Table 3 for measured *J*-couplings.

both chemical shifts are sensitive to amide conformation as shown in **1/2** (Table 1), and the easily measured $^2J_{\text{C}2,\text{C}1'}$ between both ^{13}C -labeled carbons could be used to validate C1' and C2 signal assignments in *cis* isomers.

NMR Spectra of 3 and 4. 1D ^1H NMR spectra of **3** and **4** in aqueous ($^2\text{H}_2\text{O}$) solution contained signals from the dominant *trans* amide form (Table 4). Efforts to detect and assign signals arising from the *cis* amides were unsuccessful because of their weak intensities in spectra containing significant signal overlap.

In contrast, 1D $^{13}\text{C}\{^1\text{H}\}$ NMR spectra of the doubly ^{13}C -labeled **3** and **4** contained strong doublets attributed to the

labeled C2 and exocyclic C=O (C1') carbons of the *trans* form (Figure 4). In each spectrum, identical splittings were observed in both signals due to the presence of $^2J_{\text{C}2,\text{C}1'}$, thus confirming $^{13}\text{C}2\text{--N}2\text{--}^{13}\text{C}1'$ bond connectivity. On the basis of the ^{13}C chemical shift behaviors established for **1** and **2**, a close examination was made of regions 4–6 ppm downfield of each

- (35) Mobli, M.; Almond, A. *Org. Biomol. Chem.* **2007**, *5*, 2243–2251.
 (36) (a) Church, T.; Carmichael, I.; Serianni, A. S. *Carbohydr. Res.* **1996**, *280*, 177–186. (b) Serianni, A. S.; Bondo, P. B.; Zajicek, J. *J. Magn. Reson.* **1996**, *112B*, 69–74. (c) Zhao, S.; Bondo, G.; Zajicek, J.; Serianni, A. S. *Carbohydr. Res.* **1998**, *309*, 145–152.

Table 2. $K_{trans/cis}$ for **1** and **2** at Different Solution Temperatures

T (°C)	$K_{trans/cis}$ (1 ; α)	$K_{trans/cis}$ (2 ; β)
42.0	4.22 ± 0.03^a	2.84 ± 0.02
52.7	3.95 ± 0.02	2.69 ± 0.02
58.0	3.84 ± 0.02	
64.4	3.76 ± 0.02	2.59 ± 0.02
69.7	3.64 ± 0.02	
75.1	3.54 ± 0.02	2.49 ± 0.02
84.6	3.37 ± 0.02	2.41 ± 0.02

^a Errors based on variations observed from multiple integration of ^{13}C NMR signals in a given spectral data set.

of these intense signals in an effort to detect signals arising from *cis* forms. Weak signals were detected (Table 4; Figure 4). Splittings of the C=O (C1') and C2 signals attributed to putative *cis* forms were identical, suggesting that the signals arose from carbons in the same molecule.

Further support for the *cis* and *trans* signal assignments in **3** and **4** was obtained from ^{13}C NMR spectra of the triply ^{13}C -labeled isotopomers **3'** and **4'**. In both anomers, the labeled carbons were mutually coupled, giving rise to three-spin systems containing internally consistent *J*-couplings; these results are shown for **4'** in Figure S2 in Supporting Information.

Although the *cis* signals were weak, the use of ^{13}C -labeled compounds allowed determinations of the percentages of both *cis* and *trans* amides of **3** and **4** at different solution temperatures by integration of either the labeled C1' (C=O) or C2 carbon signals (Table 5; only data for C2 are shown). In **3**, the *cis* amide varied from 1.4% to 2.5% as temperature increased from 42.0 to 84.6 °C (Table 5). In contrast, the *cis* amide varied from 1.9% to 3.1% in **4** over a temperature range of 31.3–75.1 °C. At 52.7 °C, the percentage of *cis* form was greater in **4** (2.6%) than in **3** (1.6%), showing a dependence of $K_{trans/cis}$ on anomeric configuration similar to that found for **1** and **2** (Table 2). These percentages of *cis* amide, however, are roughly 10-fold lower than found for **1** and **2** at similar solution temperatures.

Table 3. ^{13}C – ^{13}C Spin-Coupling Constants^a in **1**–**4**

cmpd	spin-coupling constant ^a								
	$^2J_{C2,C1'}$ ^b	$^3J_{C1,C1'}$	$^3J_{C3,C1'}$	$^1J_{C2,C3}$	$^2J_{C2,C4}$ ^c	$^1J_{C1',CH_3}$ (acetyl)	$^3J_{C2,CH_3}$ (acetyl)	$^1J_{C1,C2}$	$^3J_{C2,OCH_3}$ (aglycone)
1 / β - <i>cis</i>	2.8	2.1	1.0						
1 / β - <i>trans</i>	1.1	1.1	1.3						
2 / β - <i>cis</i>	2.5	1.7	1.4						
2 / β - <i>trans</i>	1.4	1.1	1.1						
3 / β - <i>cis</i>	1.1	1.6 ^d						44.7 ^d	
3 / β - <i>trans</i>	0.8	1.1	1.5	36.9	+3.0	50.3	1.6	45.0	2.8
4 / β - <i>cis</i>	0.8	1.4 ^d						44.8 ^d	
4 / β - <i>trans</i>	1.0	1.3	1.1	37.2	+2.3	50.4	1.8	45.0	3.1

^a In Hz \pm 0.1 Hz at 22 °C in $^2\text{H}_2\text{O}$. ^b Sign unknown. ^c Predicted signs based on analogous $^2J_{C2,C4}$ in β -D-glucopyranosyl rings (ref 36). ^d Couplings measured from $^{13}\text{C}\{^1\text{H}\}$ NMR spectra of **3'** and **4'**.

Table 4. ^1H and ^{13}C Chemical Shift Assignments^a for **3** and **4** in Their *Cis* and *Trans* Amide Conformations

cmpd	δ_{H1}	δ_{H2}	δ_{H3}	δ_{H4}	δ_{H5}	δ_{H6a}	δ_{H6b}	δ_{OCH_3}	$\delta_{(CO)CH_3}$
3 / β - <i>trans</i>	4.711	3.866	3.665	3.429	3.626	3.831	3.734	3.336	1.988
4 / β - <i>trans</i>	4.395	3.641	3.481	3.33–3.43	3.33–3.43	3.888	3.700	3.457	1.987
cmpd	δ_{C1}	δ_{C2}	δ_{C3}	δ_{C4}	δ_{C5}	δ_{C6}	δ_{OCH_3}	$\delta_{C=O}$	$\delta_{(CO)CH_3}$
3 / β - <i>cis</i>	101.07 ^b	60.27 ^b						179.37 ^b	
3 / β - <i>trans</i>	100.66	56.21	73.71	72.56	74.25	63.15	57.72	177.04	24.43
4 / β - <i>cis</i>	104.87 ^b	62.58 ^b						180.32 ^b	
4 / β - <i>trans</i>	104.49	58.00	76.51	72.48	78.44	63.29	59.62	177.25	24.69

^a ^1H chemical shifts in ppm relative to external dimethyl-2-silapentane-5-sulfonic acid (DSS); ^{13}C chemical shifts in ppm relative to external DSS. Measured at 22 °C in $^2\text{H}_2\text{O}$. ^b Measured from the $^{13}\text{C}\{^1\text{H}\}$ NMR spectra of **3'** and **4'**.

van't Hoff plots of the data in Table 5 gave the following $\Delta H^{\circ}_{cis \rightarrow trans}$ values: for **3**, -3.2 ± 0.4 kcal/mol; for **4**, -2.6 ± 0.2 kcal/mol. These values are slightly more negative than those found for **1** and **2**. $\Delta S^{\circ}_{cis \rightarrow trans}$ Values were also determined from van't Hoff plots, and $\Delta G^{\circ}_{cis \rightarrow trans}$ values were calculated from $\Delta H^{\circ}_{cis \rightarrow trans}$ and $\Delta S^{\circ}_{cis \rightarrow trans}$; for **3**, $\Delta G^{\circ}_{cis \rightarrow trans} = -2.7 \pm 0.1$ kcal/mol, $\Delta S^{\circ}_{cis \rightarrow trans} = -1.6 \pm 1.2$ cal/K/mol; for **4**, $\Delta G^{\circ}_{cis \rightarrow trans} = -2.4 \pm 0.1$ kcal/mol; $\Delta S^{\circ}_{cis \rightarrow trans} = -0.7 \pm 0.5$ cal/K/mol. Thus, like **1** and **2**, the conversion of *cis* \rightarrow *trans* amide is enthalpically favored and entropically disfavored in **3** and **4**.

Rate Constants for Amide *Cis*–*Trans* Isomerization in **1–**4**.** ^{13}C Saturation-transfer (^{13}C ST) experiments were conducted on **1**–**4** to test for the presence of chemical exchange and thus confirm the assignment of *cis* and *trans* ^{13}C NMR signals (Figure 4), and to measure amide *cis*–*trans* isomerization (CTI) rate constants and associated kinetic activation parameters.

Rate constants $k_{trans \rightarrow cis}$ in **1** and **2** at different temperatures, obtained from steady-state ^{13}C ST experiments (see NMR Spectroscopy section), are given in Table 6. At 64.4 °C, $k_{trans \rightarrow cis}$ for **1** was 0.15 ± 0.04 s⁻¹; this value increased \sim 5-fold to 0.77 ± 0.05 s⁻¹ at 84.6 °C. In contrast, $k_{trans \rightarrow cis}$ for **2** was 0.62 ± 0.05 s⁻¹ at 64.4 °C, increasing to 3.59 ± 0.16 s⁻¹ at 84.6 °C. The rate of conversion of *trans* \rightarrow *cis* amide depends on anomeric configuration, with conversion more favored in **2**. Energies of activation (E_{act}) for *trans* \rightarrow *cis* were 19.6 ± 3.7 kcal/mol for **1** and 19.6 ± 4.5 kcal/mol for **2**.

Rate constants $k_{cis \rightarrow trans}$ in **1** and **2** (Table 6) were calculated from $k_{trans \rightarrow cis}$ and $K_{trans/cis}$ values at each temperature. Energies of activation (*cis* \rightarrow *trans*) were 18.3 ± 3.9 kcal/mol for **1** and 18.8 ± 4.5 kcal/mol for **2**. Amide CTI appears more kinetically favored in **2** than in **1**, on the basis of the larger $k_{trans \rightarrow cis}$ and $k_{cis \rightarrow trans}$ values observed in the former at any temperature.

CTI kinetics measurements were conducted on **3** and **4** using time-dependent ^{13}C ST in which the C1' (carbonyl) carbon of the *cis* form was saturated for varying times and the effect of this saturation monitored on the C1' signal intensity of the *trans*

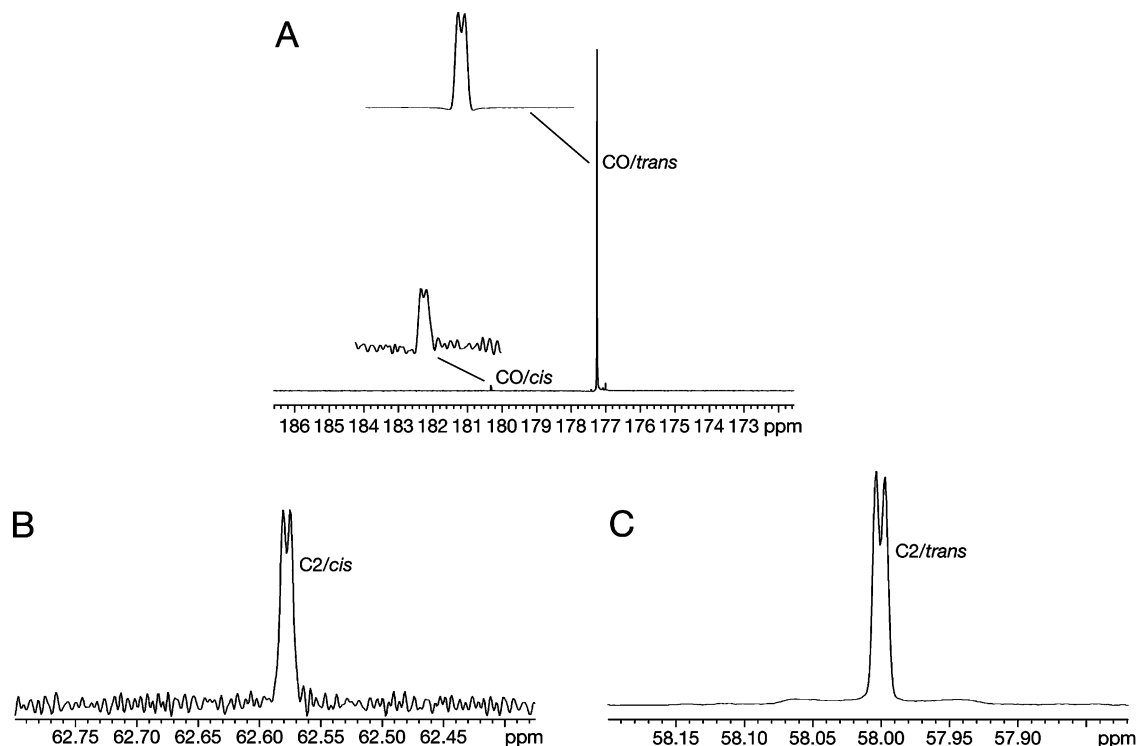


Figure 4. Partial $^{13}\text{C}\{^1\text{H}\}$ NMR spectra (150 MHz) of **4** in $^2\text{H}_2\text{O}$ at 22 °C. (A) Signals from the ^{13}C -labeled carbonyl ($\text{C1}'$) carbon from *cis* (180.32 ppm) and *trans* (177.25 ppm) forms, with insets showing splittings due to $^2J_{\text{C2,C1}'}$. (B, C) Signals from the ^{13}C -labeled C2 carbon in the *cis* (62.58 ppm) and *trans* (58.00 ppm) forms, showing $^2J_{\text{C2,C1}'}$ values internally consistent with values measured from the $\text{C1}'$ signals in A.

Table 5. $K_{\text{trans/cis}}$ for **3** and **4** at Different Solution Temperatures

T (°C)	$K_{\text{trans/cis}}$ (3 ; α) ^a	$K_{\text{trans/cis}}$ (4 ; β)
31.3		53.0 ± 1.5
42.0	72.5 ± 2.8	45.3 ± 1.1
52.7	60.3 ± 1.9	38.1 ± 0.8
64.4	51.1 ± 1.4	33.8 ± 0.6
75.1	45.3 ± 1.1	31.1 ± 0.5
84.6	38.8 ± 0.8	

^a Values were determined from the integration of the C2 signals. Errors are based on variations observed from multiple integration of C2 signals in a given spectral data set.

Table 6. Rate Constants (s^{-1}), $k_{\text{trans} \rightarrow \text{cis}}$ and $k_{\text{cis} \rightarrow \text{trans}}$, for **1** and **2** at Different Temperatures

T (°C)	1 (α)		2 (β)	
	$k_{\text{trans} \rightarrow \text{cis}}$	$k_{\text{cis} \rightarrow \text{trans}}$	$k_{\text{trans} \rightarrow \text{cis}}$	$k_{\text{cis} \rightarrow \text{trans}}$
42.0			0.09 ± 0.05	0.24 ± 0.14
52.7			0.22 ± 0.04	0.60 ± 0.12
64.4	0.15 ± 0.04	0.57 ± 0.14	0.62 ± 0.05	1.61 ± 0.14
69.7	0.22 ± 0.04	0.79 ± 0.14		
75.1	0.36 ± 0.04	1.27 ± 0.14	1.57 ± 0.08	3.92 ± 0.23
84.6	0.77 ± 0.05	2.59 ± 0.19	3.59 ± 0.16	8.66 ± 0.43

form (Figure 5A). Data linearization at different solution temperatures (Figure 5B) gave $k_{\text{trans} \rightarrow \text{cis}}$ (Table 7). For **3**, $k_{\text{trans} \rightarrow \text{cis}}$ ranged from 0.02 to 0.9 s^{-1} over a temperature range of 42.0–84.6 °C, whereas for **4**, $k_{\text{trans} \rightarrow \text{cis}}$ ranged from 0.05 to 2.6 s^{-1} over a temperature range of 31.3–75.0 °C. As found for **1/2**, $k_{\text{trans} \rightarrow \text{cis}}$ in **3/4** depends on anomeric ($\text{C1}'$) configuration, with *trans* \rightarrow *cis* conversion more favored in β -anomer **4** at all temperatures investigated. Activation energies (E_{act}) (*trans* \rightarrow *cis*) (Figure S3 in Supporting Information) were $19.2 \pm 2.8 \text{ kcal/mol}$ for **3** and $19.4 \pm 3.0 \text{ kcal/mol}$ for **4**, values similar to those found for **1** and **2**.

Rate constants, $k_{\text{cis} \rightarrow \text{trans}}$ in **3** and **4**, calculated from $k_{\text{trans} \rightarrow \text{cis}}$ and $K_{\text{trans/cis}}$ values at each temperature, are also shown in Table 7. Energies of activation (*cis* \rightarrow *trans*) were $16.0 \pm 3.2 \text{ kcal/mol}$ for **3** and $16.7 \pm 3.4 \text{ kcal/mol}$ for **4**, values statistically similar to those observed for **1** and **2**. Like **1/2**, amide CTI appears more kinetically favored in β -anomer **4** than in α -anomer **3**.

Additional activation parameters for the CTI of **1–4** are summarized in Table 8. ΔG^{\ddagger} values range from 17 to 21 kcal/mol and ΔH^{\ddagger} from 15 to 19 kcal/mol, and the signs of both parameters are positive. In contrast, ΔS^{\ddagger} values are uniformly negative, ranging from -3 to -9 cal/mol/K . ΔS^{\ddagger} values appear more negative for α -anomers **1** and **3** than for β -anomers **2** and **4**, but the large errors make this observation inconclusive.

Conclusions

N-Acetylation in biological systems is a common chemical modification that has important functional ramifications. For example, *N*-acetylation of L-lysine side chains of histones serves as a mechanism to reduce positive charge and thereby reduce electrostatic attraction between histones and their negatively charged nucleic acid binding partners.³⁷ This reduced affinity plays an active role in modulating gene expression.³⁸ In a similar vein, *N*-acetylation of 2-deoxy-2-aminosugars such as D-glucosamine 6P eliminates their charge properties and thus affects their biological behaviors and functions. For example, D-galactosamine is toxic in animals and thus is normally found in its *N*-acetylated form *in vivo* (found as UDP-GalNAc produced via C4-epimerization of UDP-GlcNAc).³⁹ In contrast, D-glucosamine 6P is synthesized *in vivo* from D-fructose 6P by the bifunctional enzyme, glutamine:fructose 6P amidotransferase (GFA1), and can accumulate without toxic effects. *In vivo* conversion of D-glucosamine 6P to *N*-acetyl-D-glucosamine 6P is catalyzed by the CoA-dependent enzyme, D-glucosamine 6P *N*-acetyltransferase (GNA1).⁴⁰

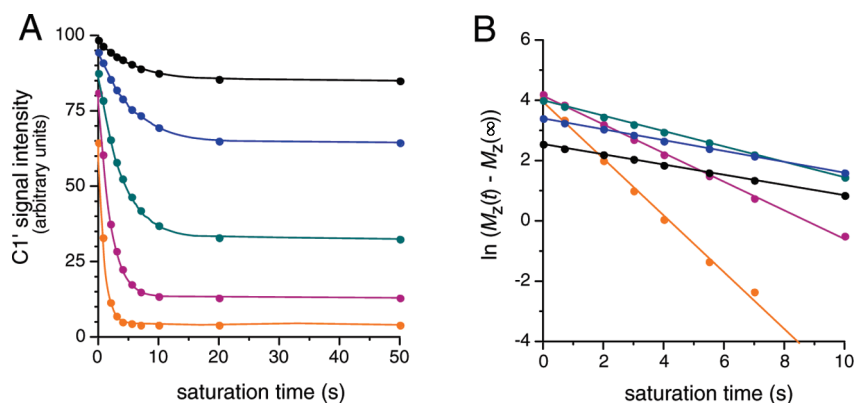


Figure 5. (A) Plots of $C1'_{trans}$ signal intensity in **3** as a function of saturation time of the $C1'_{cis}$ signal. Data were collected at different temperatures: black = 42.0 °C; blue = 52.7 °C; green = 64.4 °C; red = 75.1 °C; orange = 84.6 °C. (B) Linearization of the data shown in A following eq 1, from which $k_{trans-cis}$ values were determined.

Table 7. Rate Constants (s^{-1}), $k_{trans-cis}$ and $k_{cis-trans}$, for **3** and **4** at Different Temperatures

T (°C)	3 (α)		4 (β)	
	$k_{trans-cis}$	$k_{cis-trans}$	$k_{trans-cis}$	$k_{cis-trans}$
31.3			0.05 ± 0.02	2.58 ± 1.34
42.0	0.02 ± 0.01	1.65 ± 0.74	0.13 ± 0.02	5.70 ± 0.91
52.7	0.06 ± 0.01	3.38 ± 0.61	0.36 ± 0.01	13.7 ± 0.7
64.4	0.16 ± 0.01	8.13 ± 0.68	1.09 ± 0.01	37.0 ± 0.9
75.1	0.40 ± 0.01	17.9 ± 1.0	2.56 ± 0.01	79.7 ± 1.4
84.6	0.87 ± 0.02	33.8 ± 1.5		

Table 8. Activation Parameters for Amide *Cis-Trans* Interconversion in **1-4**

cmpd	activation parameter (<i>trans</i> \rightarrow <i>cis</i>)			
	$\ln A$	ΔG^{\ddagger} (kcal/mol)	ΔH^{\ddagger} (kcal/mol)	ΔS^{\ddagger} (cal/K/mol)
α -NFG 1	27.3 ± 5.3	20.9 ± 0.5	18.9 ± 3.7	-6.5 ± 10.4
β -NFG 2	28.8 ± 6.4	20.0 ± 0.7	18.9 ± 4.5	-3.5 ± 12.7
α -NAG 3	26.9 ± 4.0	20.7 ± 0.4	18.5 ± 2.9	-7.4 ± 7.9
β -NAG 4	28.9 ± 4.4	19.7 ± 0.4	18.7 ± 3.7	-3.2 ± 10.8

cmpd	activation parameter (<i>cis</i> \rightarrow <i>trans</i>)			
	$\ln A$	ΔG^{\ddagger}	ΔH^{\ddagger}	ΔS^{\ddagger}
α -NFG 1	26.7 ± 5.5	19.9 ± 0.6	17.6 ± 3.9	-7.7 ± 10.9
β -NFG 2	28.5 ± 6.5	19.3 ± 0.7	18.1 ± 4.5	-4.1 ± 12.9
α -NAG 3	26.0 ± 4.6	18.0 ± 0.5	15.4 ± 3.1	-9.0 ± 9.0
β -NAG 4	28.6 ± 5.0	17.3 ± 0.4	16.1 ± 3.4	-3.9 ± 9.9

Although *N*-acetylation is a ubiquitous saccharide modification in biological systems, the chemical and biochemical properties conferred by this structural change are not fully appreciated. It is well established that generic amide bonds assume both *cis* and *trans* conformations in solution, and considerable study has been directed toward understanding the thermodynamics and kinetics of amide CTI in simple systems. For example, free energy differences between *cis* and *trans* formamides and acetamides have been reported to range from 0.6 to 9.3 kcal/mol, and energy barriers to amide bond rotation in simple amides range from 18 to 30 kcal/mol depending on the nature of the substituents appended to the carbonyl carbon and amide nitrogen.⁴¹

(37) Legube, G.; Trouche, D. *EMBO Rep.* **2003**, *4*, 944–847.

(38) Verdone, L.; Agricola, E.; Caserta, M.; Di Mauro, E. *Briefings Funct. Genomics Proteomics* **2006**, *5*, 209–221.

(39) McMillan, J. M.; McMillan, D. C. *Toxicology* **2006**, *222*, 175–184.

To date, little attention has been paid to amide *cis-trans* equilibria and kinetics in *N*-acylated saccharides, specifically in GlcNAc, GalNAc, and *N*-acetyl-neuraminic acid (Neu5Ac). It is normally assumed that, in solution, the *trans* amide predominates in these and related structures, and the potential presence of *cis* isomers and their role in biology have been overlooked. The latter is especially noteworthy in light of the distribution of *cis* and *trans* GlcNAc residues in crystal structures of glycoproteins,⁴² where a broad and nearly continuous span of rotamers about the N–CO bond is observed despite the relatively high energies required to rotate the partial C–N double-bond into nonplanar conformations (*i.e.*, geometries other than the idealized *cis* and *trans* forms) (Figure 6A). This energy likely derives from crystal packing forces, highlighting the high degree of structural deformation accessible in crystal structures of conformationally flexible molecules or fragments thereof under certain packing conditions. Additional analysis of the same data set with respect to the more easily rotatable C2–N2 bond (α) shows a preference for α -*anti* (*i.e.*, H2 *anti* to NH) (Figure 6B), a result consistent with prior interpretations of $^3J_{H2,NH}$ spin-couplings in GlcNAc and related structures measured in solution.³⁵ Correlation between C2–N2 (α) and amide (β) bond conformation (Figure 6C) shows a clustering of data points near 180° for both torsions, as expected, but also a discernible horizontal clustering of points attributable to the *cis* amide over a wide range of α conformations. The distribution of torsions is more uniform for α than for β , presumably as a result of the partial double bond character of the latter that destabilizes torsions between 10° to 60° and –10° to –60°.

Prior studies have shown that aqueous solutions of *N*-formylated aminosugars contain comparable amounts of *cis* and *trans* amides.^{29–32} The small *N*-formyl hydrogen apparently stabilizes the *cis* form (relative to methyl in the *N*-acetyl derivative) by minimizing steric interactions with the proximal

(40) Hurtado-Guerrero, R.; Raimi, O. G.; Min, J.; Zeng, H.; Vallius, L.; Shepherd, S.; Ibrahim, A. F. M.; Wu, H.; Plotnikov, A. N.; van Aalten, D. M. F. *Biochem. J.* **2008**, *415*, 217–223.

(41) Isaacs, N. *Physical Organic Chemistry*, 2nd ed.; Longman Scientific and Technical: Harlow, England, 1995; p 350.

(42) This survey was conducted on 1311 pdb files (from the RCSB PDB database) containing a total of 7994 GlcNAc residues. Within the latter group, 917 residues contained a H2–C2–N2–H torsion angle between 60° and –60°, producing an ~11% α -*syn* population; the remaining ~89% is α -*trans*. More pertinent to the present work, 463 residues contained a C2–N2–C1'–C2' torsion angle between 60° and –60°, giving an ~6% β -*cis* population.

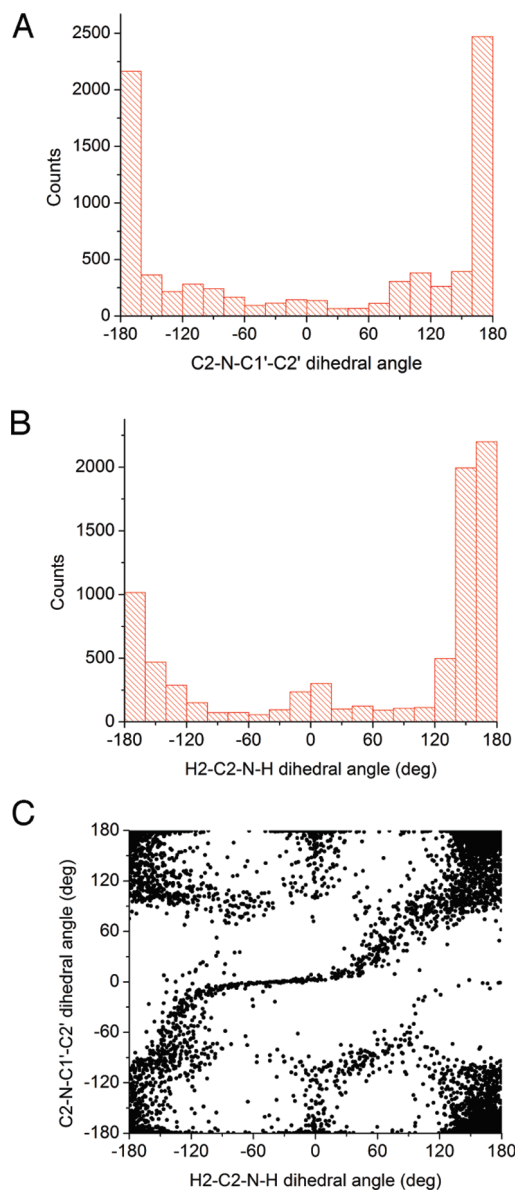


Figure 6. (A) Distribution of C2–N2–C1'–C2' dihedral angles observed in a survey of crystal structures of GlcNAc residues in glycoproteins taken from the PDB.⁴³ The *trans* amide predominates (180°), but a continuous distribution of angles is observed over the full 360° rotation, including that for the *cis* amide (0°). (B) Distribution of α dihedral angles in the same ensemble of X-ray structures as in A. (C) Correlation between conformations of the α and β bonds in the same group of GlcNAc structures sampled in A and B.

C2–H2 bond.⁴³ In the present work, NMR characterization of the *N*-formyl glycosides was a prerequisite to the more challenging detection and quantification of *cis* amide in solutions of GlcNAc glycosides. The success of the latter work hinged on the assumption that the effects of amide conformation on ^1H and ^{13}C chemical shifts for nuclei in the vicinity of the amide bond were similar in the *N*-formyl and *N*-acetyl derivatives, thus allowing signal assignments in the latter despite the low abundance of *cis* amide. While this assumption proved valid,

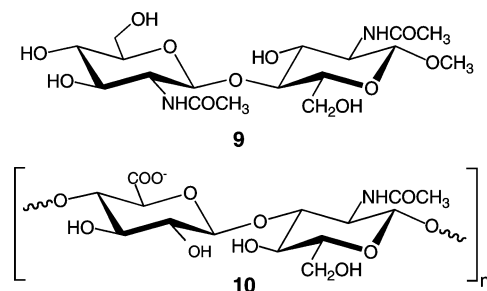
(43) Eliel and Wilen have suggested that the preference for *trans* amide conformations in solution is due to a combination of steric (attractive in *trans*, repulsive in *cis*) and charge interaction factors. See ref 44 for further discussion.

(44) Eliel, E. L.; Wilen, S. H. *Stereochemistry of Organic Compounds*; Wiley: New York, 1994; pp 620–621.

additional support for *cis* and *trans* signal assignments in **3/4** was obtained from studies of internally consistent ^{13}C – ^{13}C spin-couplings in ^{13}C -labeled GlcNAc isotopomers and by the demonstration and quantification of *cis–trans* chemical exchange by ^{13}C saturation transfer.

The equilibrium between *cis* and *trans* amides in the *N*-formyl and *N*-acetyl derivatives of methyl D -glucosaminide depends on anomeric configuration. The *cis* amide is less stable in α -anomers of NFG and NAG methyl glycosides than in the corresponding β -anomers. Given the proximity of the *N*-acyl side chain to the anomeric center in these structures, this dependency might be expected. Inspection of molecular models, however, does not provide a structural rationale for the observed dependency if preferred conformation about α in the *cis* amides is *anti* (as observed in the *trans* amides based on $^3J_{\text{H}_2,\text{NH}}$ values³⁵). On the other hand, if α is *syn* in *cis* amides, or partly so, in solution, then the acyl side chain and the axial C1–O1 bond would be in close proximity in α -anomers, thereby producing a destabilizing steric interaction.⁴⁵ This problem and the effects of acyl chain structure and length on the anomeric dependency of $K_{\text{trans/cis}}$ will require further investigation.

The relatively small rate constants for saccharide *cis–trans* isomerization call attention to the potential implications of this process in biological receptor binding and enzyme catalysis. In hypothetical cases in which the *cis* amide of GlcNAc is the productive form for binding, the overall rate of binding could be determined by the rate of conversion of the *trans* to *cis* form. Whether such a scenario occurs *in vivo* and whether biological systems have evolved enzymes to facilitate CTI in saccharides in order to circumvent this problem demand further scrutiny.



Given the importance of anomeric configuration on amide *cis–trans* equilibria in 2-deoxy-2-formamido and 2-deoxy-2-acetamido sugars, it is natural to ponder the effects of other structural perturbations on the *cis–trans* equilibria and CTI kinetics in saccharides. For example, in structures like methyl β -chitobioside **9** (and the chitin polymer derived from it) and hyaluronic acid **10**, the multiple *N*-acetyl groups may display different *cis–trans* equilibria and exchange kinetics due to their different chemical environments and/or states of solvation. Having established the fundamental NMR characteristics of *cis* and *trans* amides in simple GlcNAc glycosides, and the utility of selective ^{13}C labeling to enable such studies, it is now feasible to investigate *N*-acetyl side chain behavior in more complex

(45) Preliminary data on the behavior of α in the *cis* and *trans* forms of **2** was obtained by measuring $^3J_{\text{H}_2,\text{NH}}$ values in DMSO- d_6 solvent (Figure S4 in Supporting Information). For **2**, nearly identical coupling magnitudes were observed in both amide conformations (9.6 Hz in β -*cis*; 9.5 Hz in β -*trans*), suggesting similar bond conformations about bond α . On the other hand, the effect of amide conformation on α is probably smaller for *N*-formyl than for *N*-acetyl substituents. At present, similar J -coupling measurements have not been attempted in MeGlcNAc anomers because of the considerably less intense *cis* signals.

structures. Likewise, studies of *N*-acetyl side chain behavior in Neu5Ac, where the side chain resides in a different chemical environment than exists in GlcNAc, may reveal new structural properties that contribute to its biological properties. It is noteworthy that Neu5Ac is commonly found as a terminal (and thus exposed) residue in the oligosaccharide chains of *N*-linked glycoproteins, thus increasing the likelihood that, in some instances, recognition between Neu5Ac residues and bioreceptors may depend on side chain amide conformation.

Acknowledgment. This work was supported by a grant (to A.S.) from the National Institutes of Health (GM059239). The Notre Dame Radiation Laboratory is supported by the Office of Basic Energy Sciences of the United States Department of Energy. This is Document No. NDRL-4815 from the Notre Dame Radiation Laboratory. The authors thank Omicron Biochemicals, Inc. for gifts

of 2-amino-2-deoxy-D-[2-¹³C]glucose hydrochloride and 2-amino-2-deoxy-D-[1,2-¹³C₂]glucose hydrochloride.

Supporting Information Available: Routes for the synthesis of NFG glycosides; DFT-calculated total energies of **5–8** (*in vacuo* and solvated); ¹H–¹H spin-coupling constants in **1** and **2**; van't Hoff plots for **1** and **2**; partial ¹³C{¹H} NMR spectra of **4'**; Arrhenius plot of *k*_{trans→cis} in **4**; partial ¹H NMR spectrum of **2** in DMSO-*d*₆; description of the synthesis of **2**; description of the synthesis of **3'** and **4'**; description of calculations of kinetic activation parameters *E*_{act}, Δ*G*^{o‡}, Δ*H*^{o‡}, and Δ*S*^{o‡}; full ref 23. This material is available free of charge via the Internet at <http://pubs.acs.org>.

JA9086787